Engineering Structures 305 (2024) 117719

Contents lists available at ScienceDirect

Engineering Structures

journal homepage: www.elsevier.com/locate/engstruct

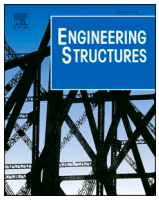

Residual stresses of MAG-welded ultrahigh-strength steel rectangular hollow sections

Lassi Keränen [a,*], Mika Pylvänäinen [b], Antti Kaijalainen [a], Tuomas Jokiaho [c], Juha Tulonen [d], Anssi Hyvärinen [d], Minnamari Vippola [e], Emil Kurvinen [a]

[a] Materials and Mechanical Engineering, University of Oulu, Finland
[b] Intelligent Machines and Systems, University of Oulu, Finland
[c] VTT Technical Research Centre of Finland Ltd, Finland
[d] SSAB Europe, Hämeenlinna, Finland
[e] Materials Science and Environmental Engineering, Tampere University, Finland

ARTICLE INFO

Keywords:
Ultrahigh-strength steel
rectangular hollow section
residual stress
MAG-welding
welding heat input
FEM simulation

ABSTRACT

Residual stresses are an important factor in the performance and stability of welded structures. This study investigates the characteristics and significance of residual stresses in MAG-welded ultrahigh-strength steel rectangular hollow sections. The research incorporates comprehensive X-ray diffraction residual stress measurements, electron backscatter diffraction analysis, statistical analyses, and finite element method simulations to provide valuable insights into the behaviour of welding residual stresses. The results reveal clear microstructural variations between the cold-formed corner and the flat side of the rectangular hollow section caused by welding heat input, emphasizing the need to consider these variations in residual stress assessments. Furthermore, the study examines the dependence of residual stresses on the steel grade, with higher strength steel exhibiting compressive stresses and lower strength materials experiencing tensile stresses in corner areas. Statistical analysis indicates that welding sequence and direction have negligible effects when applying the employed welding sequence. In any case, higher heat input leads to significantly larger residual stresses. Finally, the study presents a novel analytical model based on validated finite element simulations to predict the maximum variation of residual stresses depending on welding heat input. The findings provide valuable insights into the significance of welding residual stresses and their predictability. The comprehensive measurements, simulations and proposed models contributes to a better understanding of residual stress phenomena, facilitating the development of reliable design guidelines for welded structures in various engineering applications.

1. Introduction

As competition in the metal industry is getting fiercer, the demands of steel products and their different properties are increasing. For example, safety, performance, efficiency, high load bearing capacity, low weight and good fatigue strength are desired properties in all steel components, machines and structures. Ultrahigh-strength steels (UHSS) have been developed to meet these requirements. One of the main purposes of engineering is to produce a machine that is safe for the user and environment, which requires knowledge of operating conditions, materials and failure mechanisms [1]. Thus, the development, research and use of UHSS in mechanical engineering is well-argued.

However, the design and manufacturing guidelines and knowledge are incomplete, especially regarding the design of welded UHSS components in fluctuating operating conditions. One major unknown factor in the design of high-performance structures is the effect of welding residual stresses in ultrahigh-strength structural tubes combined with residual stresses from the tube manufacturing process. This can lead to thicker materials, which, at worst, reduces the benefits of UHSS, especially in dynamically loaded conditions. According to the IIW (International Institute of Welding) recommendations for the fatigue design of welded joints [2], the category of welding residual stresses should be evaluated by the design office; if a reliable assessment cannot be made, the worst situation must be used in fatigue design. This can lead to overconservative design because the formation and evaluation of residual stresses is not a simple topic.

* Correspondence to: Materials and Mechanical Engineering, University of Oulu, P.O. Box 8000, FI-90014, Finland.
E-mail address: lassi-pekka.keranen@oulu.fi (L. Keränen).

https://doi.org/10.1016/j.engstruct.2024.117719
Received 22 June 2023; Received in revised form 9 February 2024; Accepted 18 February 2024
Available online 24 February 2024

Welding is the most common and efficient technique to permanently join steel components made of UHSS [3]. However, the heat caused by welding changes the properties usually achieved by the thermo-mechanical manufacturing process, as shown in the previous study with S960 steel [4]. In addition to microstructural and mechanical changes, welding causes high residual stresses, affecting the welded joints' fatigue properties [5,6]. Compression residual stresses can be beneficial, but tensile residual stresses typically have a detrimental effect on fatigue strength, because they increase the mean stress in variable loading depending on the applied stress range [5,6]. In addition to this, high residual stresses may expose brittle fracture and stress corrosion and reduce the buckling strength. Residual stresses also cause distortion and inaccuracy, increasing manufacturing costs [7] and weaken the bending stiffness of pipe-sphere welded joints [8]. It has been shown that welded UHSSs are sensitive to hydrogen-induced cold cracking due to high tensile residual stress [9].

During the welding process, the weld area is heated up quickly melts materials in weld areas. The heated material expands, and the surrounding colder areas resist the expansion. The yield strength decreases when the temperature rises and the heated material partly exceeds the yield strength and is compressed plastically. After cooling, the yield strength is returned toward original strength and the compressed area is smaller than before welding, which causes tensile residual stress. Balancing compressive residual stress develops in the surrounding area. At the microstructural level, the tensile or compressive residual stress is seen as increased or decreased interplanar lattice spacing, respectively. [10].

Residual stresses can be predicted using the finite element method (FEM) based on combined thermal-mechanical analysis. In the literature, there are many alternatives to simulate welding residual stresses numerically: 2D or 3D methods, movable heat source, as Goldak's model [11], movable heat based on element birth and death [12], heat cycle method [9], simplified heat source [13] different material models depending on the phase transformation properties, typically based on temperature dependent heat capacity [5,7,12,14–17]. Ghafouri et al. [3] simulated the welding residual stresses and deformation of fillet welds made of high strength S700 MC plus steel and reported that peak stress can exceed the yield strength and the external constraints have a significant effect on the residual stresses of short welds. Sun and Dilger [9] compared a transient method with a moving heat source and a thermal cycle method for simulating the residual stresses of bead-on-plate welded S960QL UHSS. In the thermal cycle method, a predefined thermal cycle is applied to the entire length of a weld seam simultaneously, concluding that the method is not reliable at predicting the residual stresses of thick-walled UHSS, although it can reduce the calculation time. Deng et al. [13] proposed a method, where predefined thermal cycle, called simplified moving heat source, is applied to the different length portion of the pipe girth weld resulting accurate residual stresses and reasonable calculation time. Xiao et al. [18] proposed a simulation method for transverse bending and longitudinal welding, where bending is modelled by 2D elements and longitudinal welding is modelled by 3D thermo-mechanical simulation. Based on these papers, the welding residual stresses can be simulated with many methods with good accuracy. Because the residual stresses depend on the material behaviour over a wide temperature range, an accurate simulation requires expertise in material properties.

Bhatti et al. [19] studied the material properties needed in the simulation of welding residual stresses and distortion. The temperature-dependent material properties in thermal-mechanical analysis are thermal conductivity, heat capacity, thermal expansion, yield stress, elongation, Young's modulus and Poisson's ratio. Bhatti et al. [19] found that heat capacity (for calculation of temperature distribution) and yield strength (for calculation of plastic thermal deformation) are the most important temperature-dependent properties in residual stress analysis. The other properties are more important in distortion analysis and can be considered as at constant room temperature value.

Hollow sections are generally used in many weld-assembled engineering applications under variable loading: for example, as the load bearing components in buildings, bridges and machines, and in different service bridges and protecting structures. UHSS hollow sections may be manufactured from steel strips by cold roll forming. In indirect forming, a strip is first formed into a circular profile, then the longitudinal seam is welded and finally the circular profile is formed into a rectangle, while in the direct forming method, a strip is formed straight into a final cross-section [20,21]. Many variables and parameters affect on the quality and residual stresses of hollow sections: for example, forming method, forming roll sizes, number and distance of forming stands, material formability, corner radius and the hollow section's width-to-thickness ratio. The residual stress distribution is thus complicated and highly dependent on the manufacturing process [22]. A typical residual stress distribution in rectangular hollow sections is compression on the inner surface and tension on the outer surface. At the corner, the residual stresses are typically lower for rectangular hollow sections formed from round mother tube than on the flat side of the tube upon different cross sections and steel grades [20–24] For example, Somodi and Kövesdi [21] have reported surface residual stresses of S960 UHSS rectangular hollow sections (120×4, 120×6 and 150×7): on the flat sides, residual stresses are 350–550 MPa and at the corner, 100–300 MPa tensile. Yao et al. [23] reported similar results for high strength (120×4 and 200×120×5), and Li et al. [20] for conventional, steel hollow sections. In Yao et al. research [23], a whole indirect manufacturing process was noticed, so the simulation results include all residual stress sources due to manufacturing process. They showed that rectangular hollow sections have more variable residual stress distribution in corner areas than square sections. Ma et al. [25] reported residual stresses of 700, 900 and 1100 MPa grade hollow sections and they showed the cold-forming effects on tensile properties and residual stresses. Jaamala et al. [24] reported the residual stresses of S700 rectangular hollow sections and proposed a model for residual stress prediction in cold-formed rectangular hollow sections in up to S960 steels. The properties of similar S700 grade cold-formed hollow sections have been studied previously; the strength and microstructure were changed in differently formed areas [26].

The purpose of this study is to investigate the effects of MAG-welding (Metal Active Gas welding) on the residual stresses of butt-welded ultrahigh strength S700 and S960 rectangular hollow sections (RHS). This paper presents a comprehensive study of the effects of MAG-welding heat input on the microstructural changes and residual stresses, their statistical significance, and the prediction of the residual stresses of butt-welded UHSS rectangular hollow sections. The effects of MAG-welding were clarified with two different welding heat input values for both steel grades and the results were compared with the residual stresses of unwelded tubes. Altogether 215 residual stress measurements were performed based on X-ray diffraction (XRD) and results were discussed in terms of the welding sequence, welding direction and different welding heat inputs. The microstructural changes caused by welding were also reported. In the statistical analysis, for studying the effect of welding heat input and welding sequence on the residual stresses, performed using R Statistical Software (v4.2.3) [27], the uncertainty of the arithmetic mean (hereafter referred to as the mean) of the residual stresses, i.e., its 95% confidence limits, was examined at each factor level and visualized using a non-parametric bootstrap method [28]. In addition, permutation tests [29–32] were used to clarify the effect and statistical significance of the factors on the residual stresses. The analyses were performed by using maximum principal residual stresses with directions, they describe the residual stress state in a more approachable way than only longitudinal or transverse stresses. Finally, an effective model based on finite element analysis with the initial residual stress state was applied to estimate the residual stresses of butt-welded ultra-high strength steel RHS with different welding heat input levels. Measured material properties were used in the simulations. Based on the

measurements, statistical analyses and FEM simulations, a novel analytical welding heat input–residual stress model was proposed for S700 and S960 UHSS hollow sections. The proposed model provides an easy and reliable tool for assessing the welding residual stresses in rectangular UHSS hollow sections.

2. Material and methods

2.1. Test material

The studied materials were commercial S700 and S960 grade rectangular hollow sections produced by indirect cold roll forming and high frequency welding (HFW) adhering to EN 10219–3 [33] with a thickness of 4 mm and side length of 100 mm (Fig. 1). The nominal yield strengths of the materials are 700 MPa and 960 MPa. The studied tubes are cold roll formed from thermo-mechanically rolled (TMP) strip steel. The chemical compositions and nominal mechanical properties of the studied steels are shown in Table 1.

2.2. Welding

Automated MAG-welding with matching filler metals was used in this study. To achieve solid and high-quality butt-welds, we used machined V-grooves (50°) and mild steel weld root backings. The total length of the specimens after welding is 520 mm. For both materials (S700 and S960), two different welding travels speeds were used to produce two different welding heat inputs: low heat input (LQ) and high heat input (HQ). The higher heat input values correspond to the recommendations of steel manufacturer SSAB [34]. The welding parameters and heat inputs are shown in Table 2. Welding was done in four parts to minimize the welding distortions and to balance the welding residual stresses between tube corners. The welding sequence and setup are shown in Fig. 1 along with the coordinate system used in the analysis. The longitudinal HF (high frequency) welds from tube production are not covered; every mention of welding refers to butt-welds between two tubes in the study. In addition, in this paper, "BM" refers to a hollow section base material without MAG-welding.

2.3. Microstructure analysis

The microstructures of the base material and heat-affected zone (HAZ) were determined using a field emission scanning electron microscope (FE-SEM, JEOL JSM-7900 F) with electron backscatter diffraction (EBSD, Oxford AztecHKL). Acquisitions were performed at two different surfaces of RHS, in the x-y (ND-TD) and in the z-y (RD-ND) plane, which are shown in Fig. 2. The EBSD measurements were performed at an accelerating voltage of 20 kV with a step size of 0.15 μm or 0.5 μm.

2.4. Residual stress measurement

The aim of residual stress measurement is to determine the residual stress state of the unwelded and butt-welded UHSS rectangular hollow sections. In addition, we examined the effects of welding heat input on the residual stresses. Residual stress measurements were performed using an X-ray diffraction method (XRD) and XStress 3000 equipment from Stresstech Oy. XRD is a commonly used and standardized [35] non-destructive technique to determine the surface residual stresses (up to approximately 10 μm depth) of crystalline materials based on ferrite [211] plane interplanar lattice spacing according to Bragg's law on a 156° angle. The residual stresses can be calculated from the obtained strains based on the material's elastic properties, for example, according to Hooke's law. Higher lattice distance compared to stress-free distance means higher tensile residual stress. Residual stresses were measured with the Modified Chi method and the measurement parameters and setup are presented in Table 3 and Fig. 3, respectively. Measurements were taken in three directions, Φ: 0°, 45° and 90°, where 0° and 90° correspond to the tube longitudinal direction (z-axis in Fig. 1) and transversal direction (x and y -directions in Fig. 1), respectively. [36–38].

Measurements were taken around the circumference of the rectangular hollow section according to Fig. 2a. These measurements show the effect of the welding sequence on the residual stress distribution of the butt-welded tube. One tube corner includes three measurement points: point "wp1″ is the measurement point on the starting side of the weld bead, "wp2″ is a measurement point in the middle of the corner radius, and "wp3″ is the measurement point on the ending side of the weld bead. The measurement points were 2 mm, 7 mm, 15 mm, and 125 mm (rows 1–4) from the weld fusion line according to Fig. 2b. Measurements of different rows show how the welding affects residual stresses at different distances from the weld and can be utilized in FE-model verification. Measurements at 125 mm correspond to residual stresses of rectangular hollow section base material (BM) as the microstructural characterization showed at that point welding heat input have not effect on microstructure. Therefore, can be assume that 125 mm location corresponding the base material of RHS at subsurface, which includes residual stresses caused by plastic deformation from earlier processing and manufacturing.

Rows 1–3 were measured from one tube from every welding heat input group. Row 4, which means an unwelded tube, was measured from both S960 and S700 steels. In addition, row 1 was measured from one control tube from every heat input group. Four tubes were measured

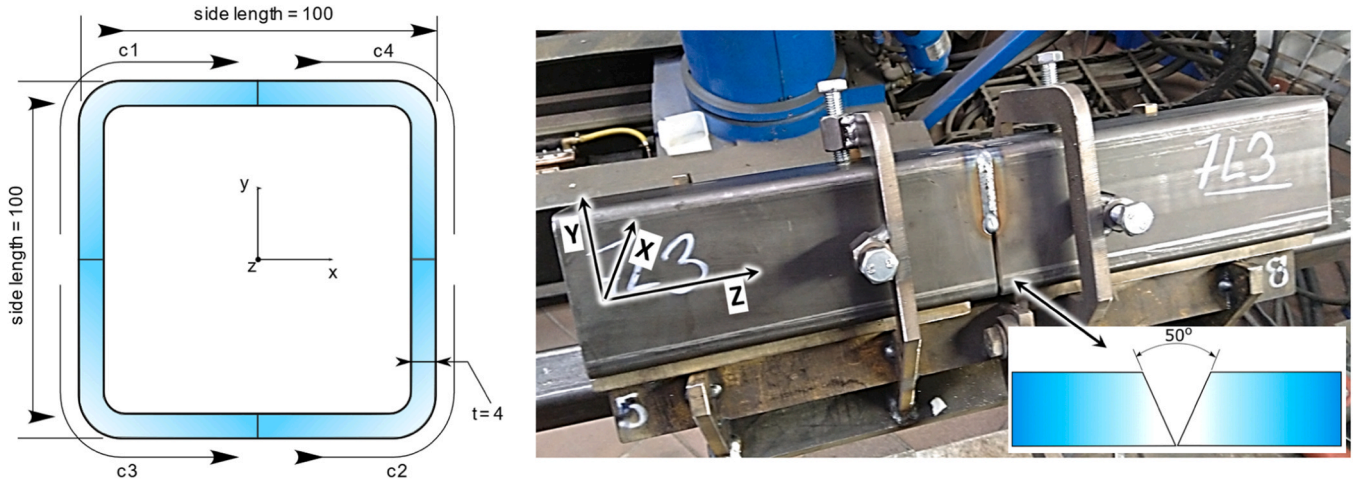

Fig. 1. Welding sequence and directions (left) and welding set-up with butt weld groove geometry (right).

Table 1
Nominal Chemical compositions and mechanical properties of S700 and S960 steels.

Material	Chemical composition [wt%]								
	C	Si	Mn	P	S	Al	Nb	V	Ti
S700	0.12	0.25	2.10	0.02	0.01	0.015	0.09	0.2	0.15
	Yield strength min [MPa]		Tensile strength [MPa]		Charpy V min impact energy		Elongation A min		CEV
	700		750–950		27 J / − 50 °C		10%		0.37
S960	0.12	0.25	1.20	0.02	0.01	0.015	0.05	0.05	0.07
	Yield strength min [MPa]		Tensile strength [MPa]		Charpy V min impact energy		Elongation A min		CEV
	960		980–1250		40 J/ − 20 °C		6%		0.48

Table 2
Welding parameters and heat input.

	700 HQ	700 LQ	960 HQ	960 LQ
Q [kJ/mm]	0.54	0.44	0.49	0.39
I [A]	165			
U [V]	21.8			
v [mm/min]	320	390	350	440
Filler metal	Esab OK Aristorod 69		Esab OK Aristorod 89	
Shield gas	Mison 25			

more specifically, and four tubes were control specimens. Altogether, 215 measurements were taken. The examined specimens and measurement points are compiled in Table 4.

2.5. Statistical analysis

The mean of the residual stresses at each factor level was calculated using data obtained from the residual stress measurements taken from the test specimens. The uncertainty of the mean, i.e., its 95% confidence limits, were calculated using a non-parametric bootstrap method which does not assume anything about the shape of the data distribution [28,39]. In the bootstrap method, the total number of stress values measured at each factor level is drawn repeatedly, 10^5 times, with replacement. From each of these resampled, i.e., bootstrapped, datasets, the mean value is calculated and stored. The 2.5th and 97.5th percentiles calculated from the stored mean values form the 95% confidence limits of the mean. The statistical significance of the factors affecting the residual stresses was calculated using a permutation test. The permutation test is a non-parametric test, and unlike parametric tests, it does not make any background assumptions about the data, i.e., it is not sensitive to the shape of the data distribution and outliers in the data. Two-sample permutation t-tests for equal variances [29] were performed for two-level factors with data of equal variance. Two-sample permutation t-tests for unequal variances [30,31] were performed for two-level factors with data of unequal variance. The statistical significance of the effect of the factors with more than two levels affecting residuals stresses

Table 3
Measurement parameters for XStress 3000.

Parameter	Value	Parameter	Value
Measurement directions, Φ*	0°, 45°, 90°	Young's modulus	211 GPa
Tilt angles Ψ (side / side)* *	5 / 5	Poisson's ratio	0.3
Max. tilt angle* *	45°	X-ray voltage	30 kV
Collimator	⌀ 3 mm	X-ray current	6.68 mA
Radiation	Cr	Exposure time	4 s

* Direction compared to Z-axis: 0° is longitudinal and 90° is transverse direction
** Tilt angle means angular deviation from the perpendicular direction of the surface

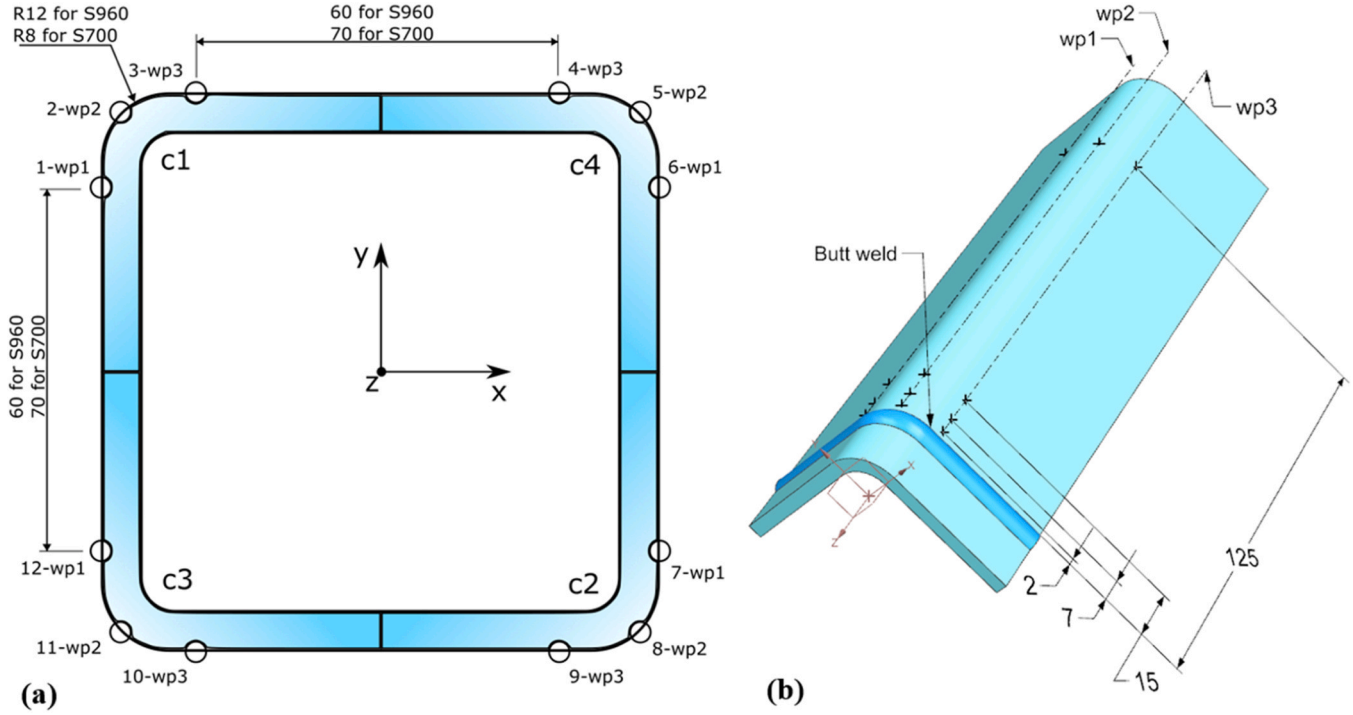

Fig. 2. Measurement points and welding points (wp) at different distances from weld (a) and measurement points of one tube corner with distances from butt-weld, where 125 mm corresponds to the unwelded base material of the rectangular hollow section (b).

Fig. 3. Residual stress measurement of tube corner using Stresstech XStress 3000.

Table 4
Specimens and measurement points.

Material	Specimen (heat input)	Number of measurement points at different distances from weld fusion line (seeFig. 2)			
		2 mm	7 mm	15 mm	125 mm, BM
700	LQ- 1	12	12	12	12
	HQ-4	12	12	12	-
	LQ-5 (control)	12	-	-	-
	HQ-3 (control)	12	-	-	-
960	LQ-2	12	12	12	12
	HQ-6	12	12	12	-
	LQ-3 (control)	12	-	-	-
	HQ-4 (control)	12	-	-	-

was calculated using a permutation test for one-way ANOVA (Analysis of Variance) [32]. In both the two-sample permutation t-test and the permutation test for one-way ANOVA, the effect of the tested factor on the residual stresses is considered significant if the *p*-value is less than or equal to 0.05.

2.6. FEM simulation of welding residual stresses

The purpose of FEM simulation is to find an efficient method for predicting welding residual stresses of ultrahigh-strength RHS considering the residual stresses induced by previous manufacturing operations. The welding residual stresses were simulated based on coupled thermal-mechanical analysis using Abaqus software [40,41]. The most important material properties used in the simulations are shown in Fig. 4. Mechanical properties, such as Young's modulus, temperature dependent yield strength and elongation up to 1000 °C for unwelded S700 and S960 steels, were obtained in previous research [42] and other properties from Eurocode 3 [43] and Nedoseka's book [44]. The engineering yield strength and elongation were converted to true values for accurate calculations [45,46]. True uniform strains are shown in Fig. 4. The isotropic hardening rule was applied in the calculations, although it can overestimate the residual stresses [14]. Heat capacities between 20 °C and 1200 °C of S700 and S960 steels were measured based on a differential scanning calorimetry (DSC) method according to ASTM E1269–11 [47]. Obtained heat capacities are shown in Fig. 4. In addition, we used the following values in our calculations: density 7850 kg/m^3, thermal expansion coefficient 1.6e-5/°C, conductivity 27.3, emissivity 0.9, convection coefficient 19 W/m^{2}K and Stefan Bolzmann constant 5.67e-8 W/m^{2}K^4.

The moving heat source was modelled based on a simplified heat source model and an element birth and death method, where the heat source is modelled as volumetric body heat flux depending on welding heat input and the volume of the weld segment. This method was chosen because the volumetric heat source method is more applicable when the weld geometry is more complicated [13,14]. The cross section of the weld was based on the groove geometry with a 50° groove angle and 1 mm reinforcement. The duration of the heating period is based on the length of weld segment and welding travel speed so that heat flux corresponds the actual heat input. In welding simulations, a quarter of the rectangular hollow section was modelled by using symmetry boundary conditions to simplify the model and reduce calculation time. Additionally, the half model was tested and produced similar results to the quarter model. It should be noted that the use of the quarter model does not consider the effects of longitudinal weld on the final residual stress state; the longitudinal HF weld may even reduce residual stresses in the welding zone [21]. Linear 8-node (C3D8RT) solid brick elements with

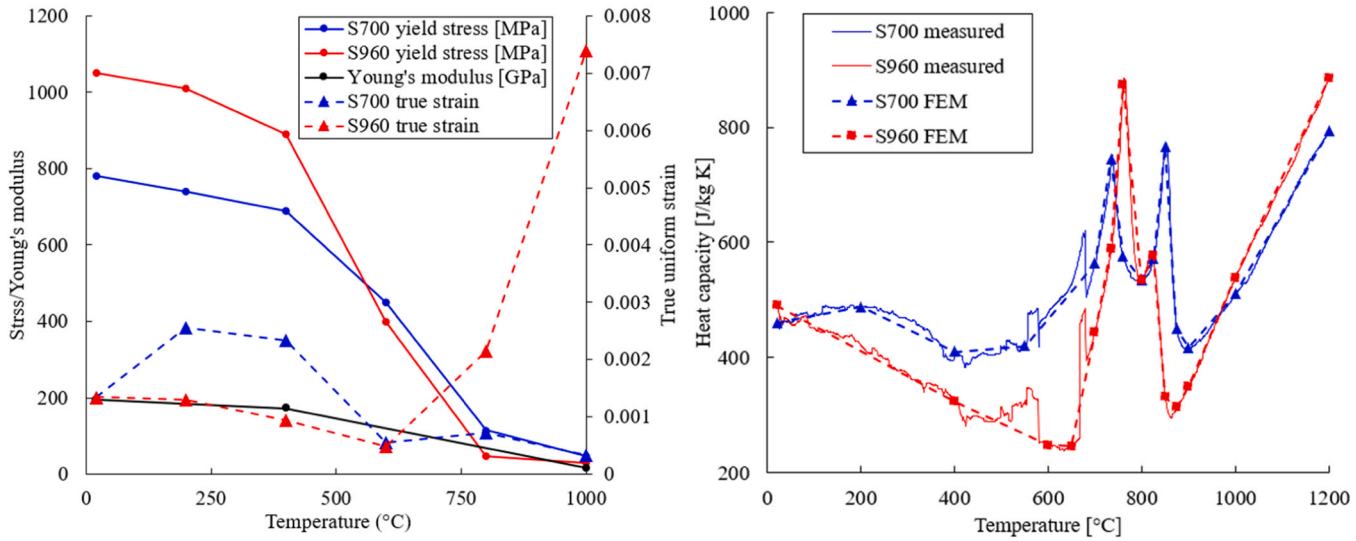

Fig. 4. Temperature dependent material properties used in simulations.

reduced integration were used in the three-dimensional coupled temperature-displacement analysis. The minimum element size was 2 mm and element size increased away from the weld. The mesh density was selected based on stress level change less than 5 MPa in loaded area while making the mesh finer incrementally. The element mesh and boundary conditions are shown in Fig. 5. The residual stresses from hollow section manufacturing were included in the simulation model as a predefined stress field. The magnitudes of predefined stresses are based on measurements of unwelded (BM) hollow sections according to the observations of this paper.

3. Results and discussion

3.1. Microstructure

The microstructure of the investigated S700 consisted of mainly polygonal ferrite, while the S960 consisted of bainite. Examples of microstructures beneath the corner and flat side surfaces of high heat input S960 hollow sections are shown in Figs. 6 and 7. In both investigated materials, the base material corners of hollow sections showed the presence of deformed grains prior to cold forming at subsurface (e.g., S960 in Fig. 6a). In Fig. 6b, on the flat side (approximately 10 mm from the center of the corner), there is no trace of cold deformation and it appears to be a typical S960 surface microstructure. While the near of weld joint, the cause of the heat-affect zone (HAZ), the bainitic microstructure is much finer and obviously the effect of cold deformation is no longer present.

The images of the flat side in the z-y (RD-ND) plane shows the HAZ and base material microstructures at the subsurface (Fig. 7). Fig. 7a clearly shows the mixtures of different heat-affected zones [i.e., coarse grained (CG, Fig. 7c), fine grained (FG) and intercritic (IC, Fig. 7d)], while Fig. 7b and e present the base material subsurface microstructure. In this study, the microstructural characterization showed that, after approximately 4 mm from the weld joint, the welding heat input has no effect on the microstructural features for S700 and S960 materials. As the microstructural features vary, especially in the HAZ, it should be considered in residual stress comparisons.

3.2. Residual stresses

A summary of the residual stress measurements is shown in Fig. 8 for S700 and S960 steels as mean values. Residual stresses are presented as maximum principal stress, which is calculated from stresses at 0°, 45°, and 90° angles. Maximum principal stress was used because it includes both the magnitude and direction of the stress on the measured plane. The mean values for maximum principal residual stresses and their directions are shown in Tables 5 and 6, respectively. The results at a 2 mm distance are calculated from two measured specimens. More detailed measurements can be found in the Appendix.

Based on the mean values in Fig. 8a, the trend of the maximum principal residual stresses on the corner (wp2) and flat side (wp1 and wp3) of the S700 tube is quite similar when the distance increase from the weld. Near to the weld (2 mm), the residual stresses on flat side are tensile, but corner is compressed. When the distance increased to 7 mm, the stresses on both measurement areas are compressive. Between 7 mm and 15 mm, residual stresses increased towards zero, except for S700 HQ, which is tensile at 15 mm. This trend is typical for welded joints; there is higher residual stress close to the weld and compressive stress on the surrounding material according to previous research. After 15 mm, residual stress levels continue to rise to the level of the base material. Based on Fig. 8a, higher welding heat input (HQ) seems to cause higher residual stresses compared to lower welding heat input (LQ). It is noticeable that stresses caused by welding are lower than for unwelded RHS (BM), both on the corner (wp2) and flat side (wp1&3) areas. This can be due to the RHS manufacturing process, when the heat induced by welding partly releases the stress from cold forming locally and develops its own stress state.

As shown in Fig. 8b, the trend of S960 residual stresses on the tube flat sides (wp1&3) are similar to the stresses of S700 tubes. The minimum and compressive residual stresses are at a 7 mm distance from the weld fusion line. On the corner area (wp2), the trend from weld to base material is downward, as shown in Fig. 8b. The residual stress on the corner area (wp2) is near to zero close to the weld, and when distance increases, residual stresses become more compressive (negative values) until they reach BM level. Typically, the residual stress caused by bending is tensile on the outer surface of the corner. Detected compressive stress on the tube corner may be due to heavy roll forming or correction of the distorted cross-sectional shape during RHS manufacturing, for example. Based on the mean values of obtained residual stresses, it can be concluded that lower heat input produces lower maximum principal residual stresses for S700 and S960 hollow sections.

Obtained maximum principal residual stresses at BM areas are compared to transverse and longitudinal residual stresses of cold-formed RHS' from literature [21,24,25] in Figs. 8c and 8d, respectively. As shown in Figs. 8c and 8d, transverse residual stresses may vary more than longitudinal stresses. Common to transverse residual stresses is that the magnitude of the stress is lower in a corner areas. Also, this variation may be due to the manufacturing and correction of distorted cross-section shape. The behaviour of longitudinal residual stress seems to be clearer between flat side and corner: longitudinal residual stress levels on the flat side are higher than on corner area for all specimens. Based on the comparison, seems that the transverse residual stress is more sensitive on deviation of the manufacturing process.

The directions of the maximum principal residual stresses for S700 RHS are shown in Fig. 9a and in Table 6 as mean values. The mean values of the maximum principal stress directions are calculated compared to butt-weld longitudinal (90°) direction; the measurements are tabulated in the Appendix. As shown in Fig. 9a, the increasing trend

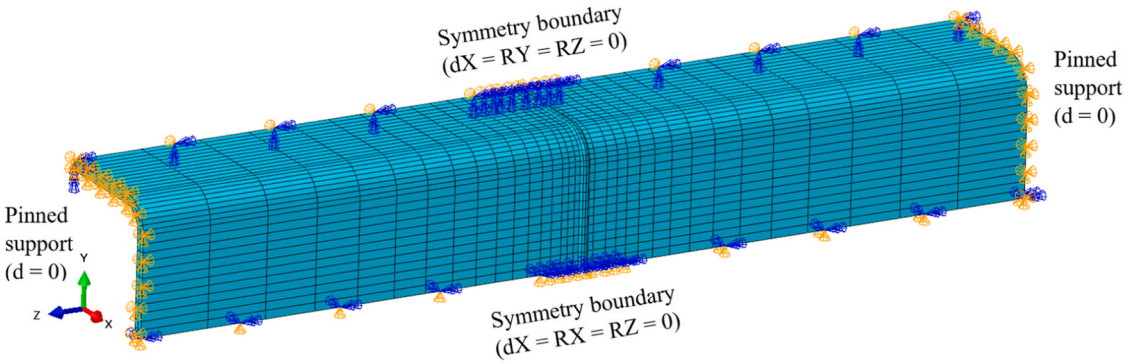

Fig. 5. Element mesh (element number 2856) and mechanical boundary conditions: orange mark is constrained displacement (d) and blue is rotation (R) degree of freedom.

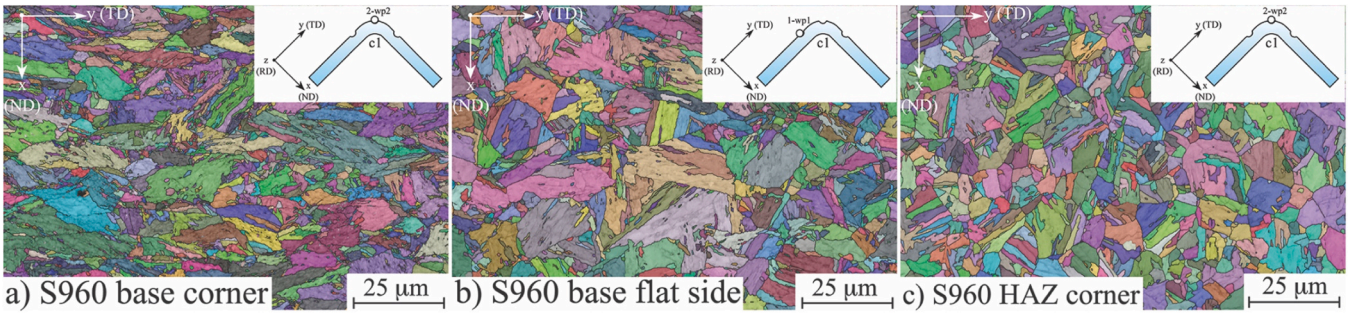

Fig. 6. ESBD grain maps (random colouring with band contrast) with high-angle (15°–62.7°, black) boundaries. Microstructures of a) base corner material, b) base flat side and c) HAZ corner of S960-HQ rectangular hollow section at ~200 μm beneath the surface in the x-y (ND-TD) plane.

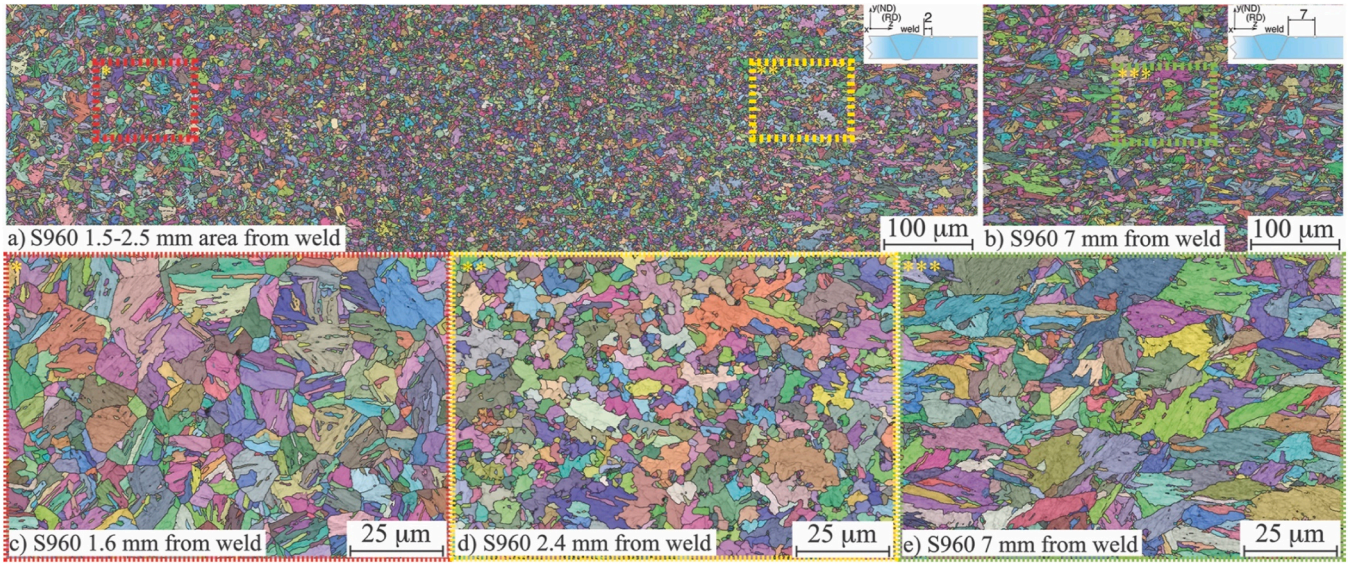

Fig. 7. ESBD grain maps (random colouring with band contrast) with high-angle (15–62.7°, black) boundaries. Microstructures a) 2 mm and b) 7 mm from the weld and the close-up of images c) 1.6 mm, d) 2.4 mm and e) 7 mm from the weld of S960-HQ rectangular hollow section at ~200 μm beneath the surface in the z-y (RD-ND) plane.

from 0–10° to 70° is similar for all measured areas of an S700 tube when distance from the weld increases. This means that the direction of the maximum principal residual stress near to the weld is somewhat parallel with MAG-welded butt-weld and the direction turns transversely away from the weld. Because the direction turns from transverse to longitudinal while distance from the butt weld increase, the direction of maximum principal residual stresses caused by tube forming is more longitudinal than transverse. This means that the residual stress state on the corner area (wp2) of S700, cold-roll formed RHS, does not correspond to the residual stress state of bended plate when the principal stress direction on bended plate is considered transverse to the bended corner. The effect of welding heat input (LQ and HQ) on the direction of residual stresses is not so clear, unlike magnitude of residual stresses, but it is clear that welding affects the direction of maximum principal residual stresses according to the theory. As shown in Fig. 9b, the trend of maximum principal residual stress of the S960 flat side (wp1&3) is a similar direction to S700 RHS. The direction changes from 0–10° to 70° when distance from the weld fusion line to the unwelded tube increases. At the corner areas (wp2), the directions near to the weld are about 0–10° but also in BM, the maximum principal residual stress direction is about 30° and more parallel with the butt-weld than it is on the flat side and S700 tubes.

In the more detailed design of UHSS structures, the magnitudes and directions of residual stresses should be taken into account; different manufacturing operations produce different residual stresses. Based on available design guidelines [2], the residual stress category should be evaluated by the design office on a case by case. One method for evaluating the final residual stress state is to use maximum principal residual stress and the direction of it, which contains both longitudinal and transverse residual stress components. Thus, especially with most critical and variable loaded welded joints, the design, welding and inspection of the welded RHS and corner areas should be performed with special care to produce high-quality and durable UHSS structures.

3.3. Statistical analysis

Statistical analysis was performed for maximum principal stresses measured at 2 mm from the weld. Measurements were taken from two tubes according to Table 4. One missing measurement point (9LQ-c1–3-3) was replaced with the mean value of the corresponding welding points of corners c2 −c4. The results of the analysis for steel grades S700 and S960 are summarized in Tables 7–10 and visualized in Figs. 10 and 11. The purpose of the analysis was to estimate the effect of the following factors on the maximum principal stresses and to determine their statistical significance using hypothesis tests. The analysed factors were: heat input (Table 7, Fig. 10a), welding direction defined by wp1 and wp3 (Table 8, Fig. 10b), welding sequence defined by c1 −c4 (Table 9, Fig. 11a), and heat input compared to the unwelded section (Table 10, Fig. 11b). These tables and figures show the mean of the maximum principal stress with a 95% confidence interval by the levels

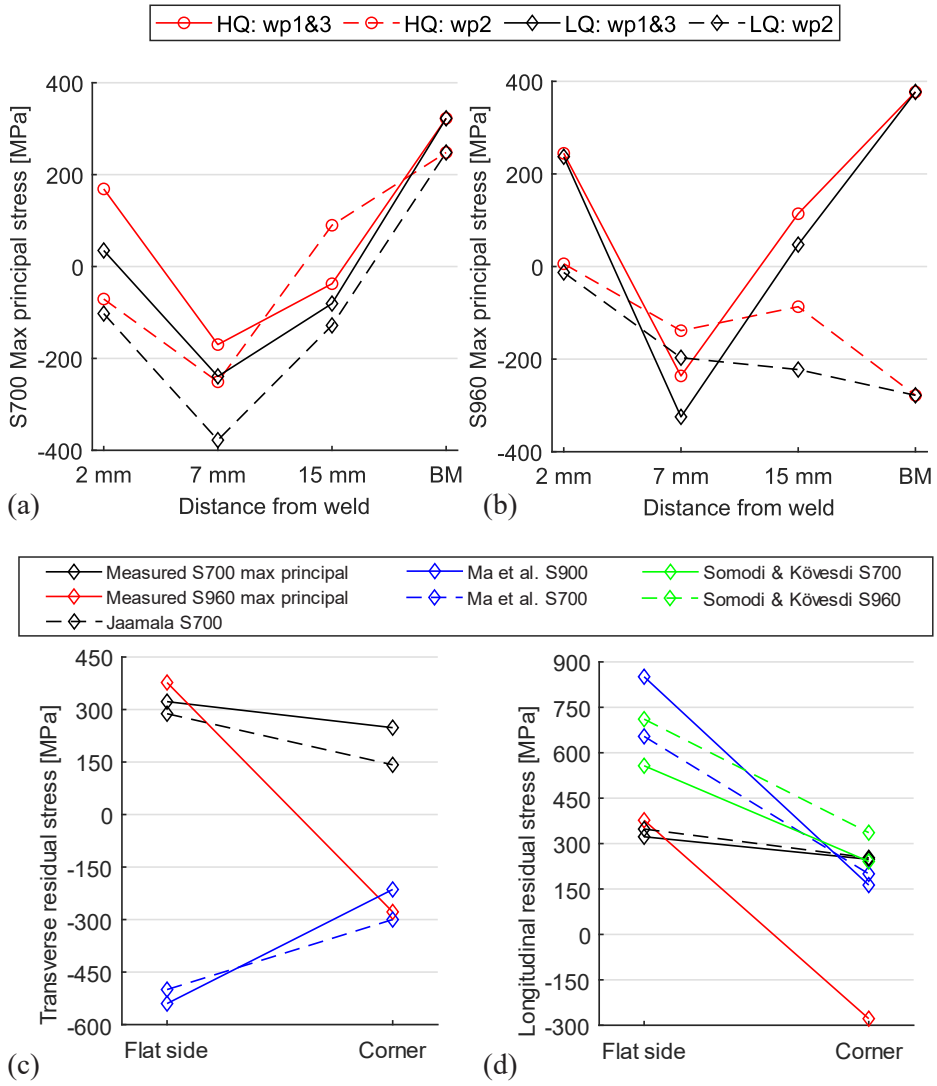

Fig. 8. Mean of the measured maximum principal residual stresses for S700 (a) and S960 (b) hollow sections, and comparison of unwelded (BM) hollow sections: transverse (c) and longitudinal (d) residual stresses with measured principal stresses.

Table 5
Mean of maximum principal stresses.

Specimen		Maximum principal residual stress [MPa]			
	Welding point	2 mm	7 mm	15 mm	125 mm, BM
700 HQ	1 & 3	168.89	-169.86	-37.46	322.52
	2	-70.74	-250.98	89.83	248.13
700 LQ	1 & 3	34.89	-239.11	-80.63	
	2	-102.4	-377.8	-128.2	
960 HQ	1 & 3	244.5	-236.3	114.0	377.1
	2	5.9	-138.6	-86.8	-278.2
960 LQ	1 & 3	237.1	-324.7	47.3	
	2	-12.9	-197.0	-222.6	

Table 6
Mean of maximum principal stress direction from butt-weld, longitudinal.

Specimen		Maximum principal stress [MPa]			
	Welding point	r1 (2 mm)	r2 (7 mm)	r3 (15 mm)	Unwelded BM, r4
960 HQ	1 & 3	3.79	20.76	56.71	74.03
	2	5.53	3.53	27.63	26.95
960 LQ	1 & 3	3.09	28.89	64.24	
	2	9.3	9.15	17.9	
700 HQ	1 & 3	10.58	25.39	45.11	66.71
	2	2.21	4.68	45.83	69.6
700 LQ	1 & 3	6.16	12.63	49.22	
	2	1.76	10.33	52.43	

of the factors under study. The tables also contain the results of the hypothesis tests, whose null hypotheses (H_0) and alternative hypotheses (H_a) were set based on a general assumption about the factors under investigation. A significance threshold of 0.05 was used in the hypothesis tests. In this work, the importance of statistical analysis was emphasized because the conclusions related to the research questions were made based on a small number of sample measurements. Although the hypothesis test may show that the factor effect is insignificant, the effect may become significant if more sample measurements were available. This, in turn, may affect the conclusions related to the research questions. Table 7 summarizes the effect of welding heat input on maximum principal stresses at welding points wp1 & wp3 and wp2. Based on the *p*-values of 0.000 and 0.037 from hypothesis tests 1 and 2 in Table 7, it can be concluded that higher HI only produces greater residual stresses in S700 steel grade. The *p*-values of 0.365 and 0.364 in hypothesis tests 3 and 4 indicate that the same conclusion cannot be drawn for S960 steel grade, although the mean values of the principal

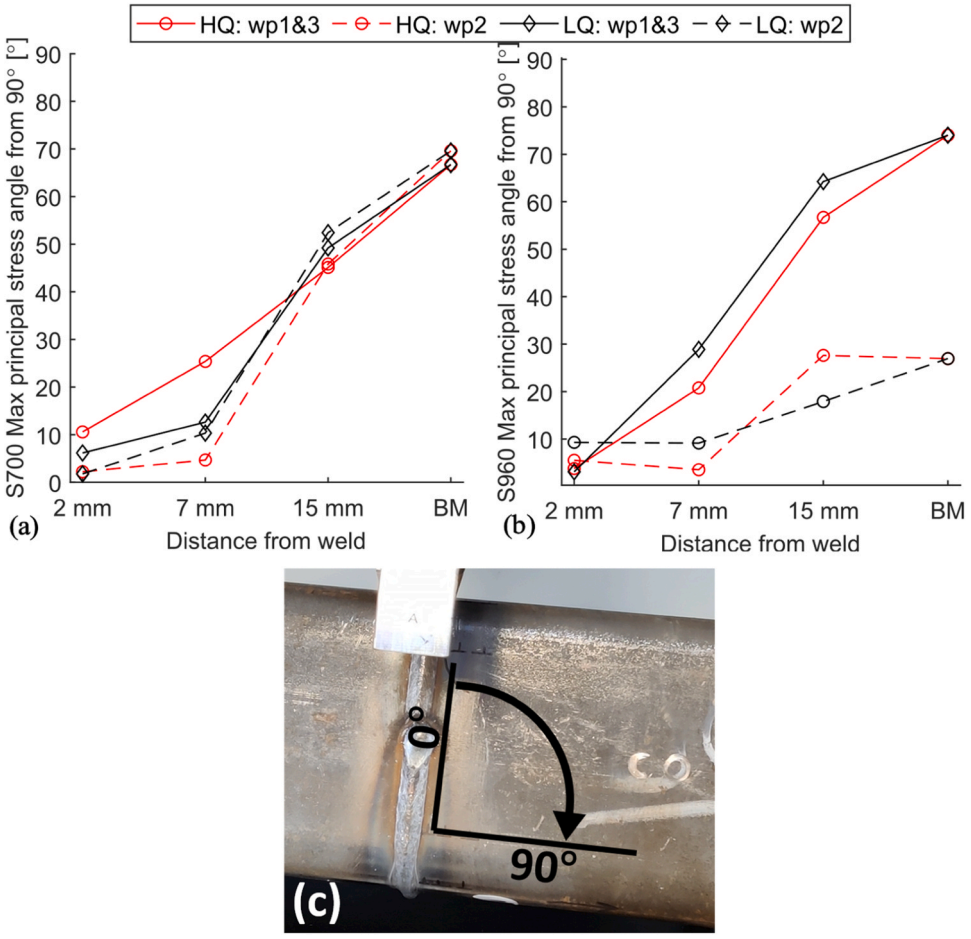

Fig. 9. Mean of the maximum principal stress direction; differences from butt-weld longitudinal direction for S700 (a) and S960 (b) hollow sections, and determining the direction (c).

Table 7
Mean of the maximum principal residual stresses with a 95% confidence interval (CI) by heat input. The table contains the results of hypothesis test between heat inputs. Hypotheses: H_0 $\mu_{LQ} \geq \mu_{HQ}$, H_a $\mu_{LQ} < \mu_{HQ}$.

Row number	Steel grade	Welding point	Heat input	Number of samples	Mean of maximum principal residual stress [MPa] (95% CI)		Hypothesis test		
							Test ID	*p*-value	Conclusion
1	S700	1 & 3	LQ	16	58.18	(−15.50 to 125.20)	1	0.000	$\mu_{LQ} < \mu_{HQ}$
2	S700	1 & 3	HQ	16	190.00	(172.20 to 208.30)			
3	S700	2	LQ	8	-102.34	(−141.90 to −63.40)	2	0.037	$\mu_{LQ} < \mu_{HQ}$
4	S700	2	HQ	8	-49.17	(−80.60 to −18.60)			
5	S960	1 & 3	LQ	16	233.38	(188.90 to 278.80)	3	0.365	$\mu_{LQ} \geq \mu_{HQ}$
6	S960	1 & 3	HQ	16	244.42	(203.40 to 283.10)			
7	S960	2	LQ	8	-12.90	(−87.70 to 68.40)	4	0.364	$\mu_{LQ} \geq \mu_{HQ}$
8	S960	2	HQ	8	5.95	(−51.30 to 64.60)			

Table 8
Mean of the maximum principal residual stresses with a 95% confidence interval (CI) by welding point. The table contains the results of hypothesis test between welding points. Hypotheses: H_0 $\mu_{wp1} = \mu_{wp3}$, H_a $\mu_{wp1} \neq \mu_{wp3}$.

Row number	Steel grade	Heat input	Welding point	Number of samples	Mean of maximum principal residual stress [MPa] (95% CI)		Hypothesis test		
							Test ID	*p*-value	Conclusion
1	S700	LQ	1	8	54.10	(−78.05 to 174.00)	1	0.916	$\mu_{wp1} = \mu_{wp3}$
2	S700	LQ	3	8	62.30	(−6.25 to 117.00)			
3	S700	HQ	1	8	199.00	(175.11 to 224.00)	2	0.353	$\mu_{wp1} = \mu_{wp3}$
4	S700	HQ	3	8	181.00	(156.70 to 206.00)			
5	S960	LQ	1	8	291.20	(225.56 to 346.00)	3	0.015	$\mu_{wp1} \neq \mu_{wp3}$
6	S960	LQ	3	8	175.60	(141.43 to 215.00)			
7	S960	HQ	1	8	254.00	(191.50 to 310.00)	4	0.652	$\mu_{wp1} = \mu_{wp3}$
8	S960	HQ	3	8	234.90	(183.31 to 285.00)			

Table 9
Mean of the maximum principal residual stresses with a 95% confidence interval (CI) by corner. The table contains the results of hypothesis test between corners. Hypotheses: H_0 $\mu_{c1} = \mu_{c2} = \mu_{c3} = \mu_{c4}$, H_a not all expected values are the same.

Row number	Steel grade	Heat input	Corner	Number of samples	Mean of maximum principal residual stress [MPa] (95% CI)		Hypothesis test		
							Test ID	*p*-value	Conclusion
1	S700	LQ	1	6	-75.12	(−162.18 to 12.30)	1	0.074	$\mu_{c1} = \mu_{c2} = \mu_{c3} = \mu_{c4}$
2	S700	LQ	2	6	-8.22	(−89.50 to 79.20)			
3	S700	LQ	3	6	30.15	(−97.20 to 152.40)			
4	S700	LQ	4	6	71.88	(−42.87 to 184.10)			
5	S700	HQ	1	6	113.97	(26.12 to 194.50)	2	0.500	$\mu_{c1} = \mu_{c2} = \mu_{c3} = \mu_{c4}$
6	S700	HQ	2	6	156.53	(67.18 to 243.40)			
7	S700	HQ	3	6	83.93	(−2.07 to 152.30)			
8	S700	HQ	4	6	86.67	(−17.83 to 185.30)			
9	S960	LQ	1	6	174.82	(91.62 to 256.60)	3	0.505	$\mu_{c1} = \mu_{c2} = \mu_{c3} = \mu_{c4}$
10	S960	LQ	2	6	192.20	(49.85 to 314.30)			
11	S960	LQ	3	6	97.47	(−5.86 to 194.70)			
12	S960	LQ	4	6	140.67	(−16.35 to 280.70)			
13	S960	HQ	1	6	217.82	(116.23 to 310.30)	4	0.186	$\mu_{c1} = \mu_{c2} = \mu_{c3} = \mu_{c4}$
14	S960	HQ	2	6	203.37	(96.57 to 294.60)			
15	S960	HQ	3	6	103.48	(−10.52 to 200.50)			
16	S960	HQ	4	6	135.07	(20.55 to 247.70)			

Table 10
Mean of the maximum principal residual stresses with a 95% confidence interval (CI) by heat input. The table contains the results of hypothesis test between heat inputs. Hypotheses: H_0 $\mu_{BM} \leq \mu_{HQ}$, H_a: $\mu_{BM} > \mu_{HQ}$.

Row number	Steel grade	Welding point	Heat input	Number of samples	Mean of maximum principal residual stress [MPa] (95% CI)		Hypothesis test		
							Test ID	*p*-value	Conclusion
1	S700	1 & 3	BM	8	362.84	(275.00 to 449.09)	1	0.000	$\mu_{BM} > \mu_{HQ}$
2	S700	1 & 3	HQ	16	190.00	(172.21 to 208.28)			
3	S700	2	BM	4	255.62	(229.05 to 282.20)	2	0.000	$\mu_{BM} > \mu_{HQ}$
4	S700	2	HQ	8	-49.17	(−80.64 to −18.65)			
5	S960	1 & 3	BM	8	377.06	(342.87 to 411.20)	3	0.000	$\mu_{BM} > \mu_{HQ}$
6	S960	1 & 3	HQ	16	244.42	(203.41 to 283.06)			
7	S960	2	BM	4	-278.23	(−304.63 to −250.00)	4	0.998	$\mu_{BM} \leq \mu_{HQ}$
8	S960	2	HQ	8	5.95	(−51.46 to 64.00)			

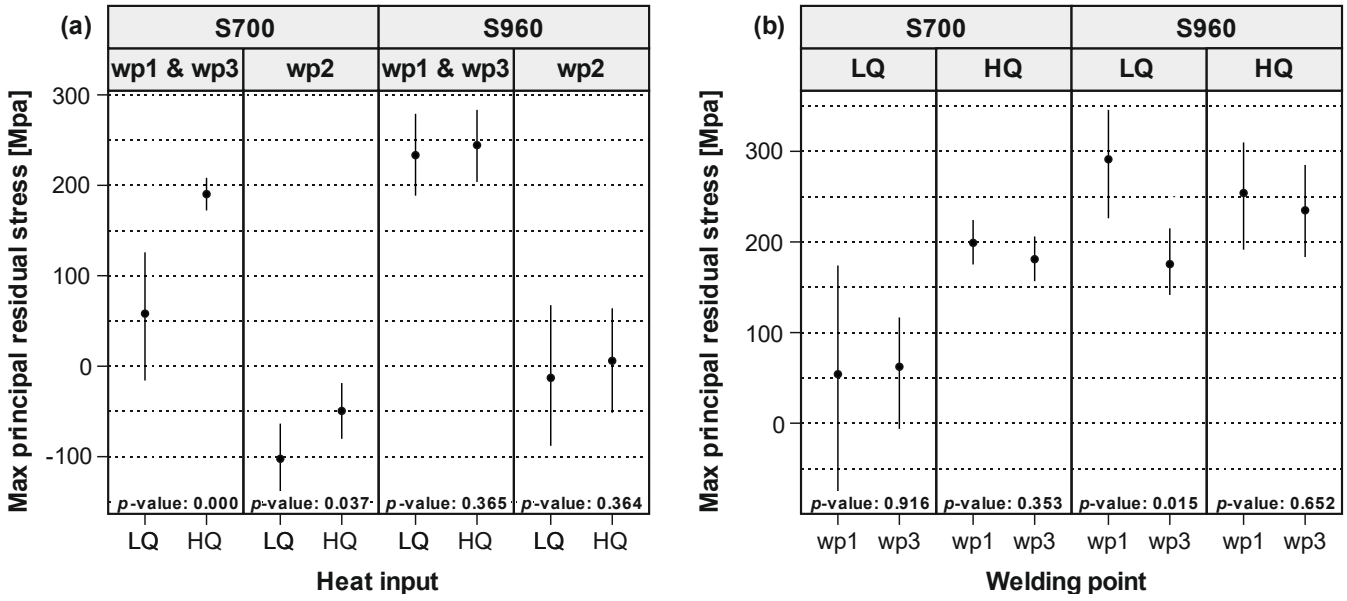

Fig. 10. Mean (black dots) of the maximum principal residual stresses with 95% confidence intervals (vertical lines through the dots) by a) heat input and b) welding point.

stresses with HQ are greater than the corresponding values with LQ. This is due to the small differences between mean values relative to the range of their 95% confidence intervals. The behaviour of the maximum principal residual stresses described above is displayed in Fig. 10a, which also reveals the difference in maximum principal stresses between the groups of welding points 1&3 and welding point 2 in both steel grades.

Table 8 summarizes the effect of welding direction on maximum principal stresses of welded corners with LQ and HQ heat input. Based on the *p*-value of 0.015 for hypothesis test 3 in Table 8, it can be

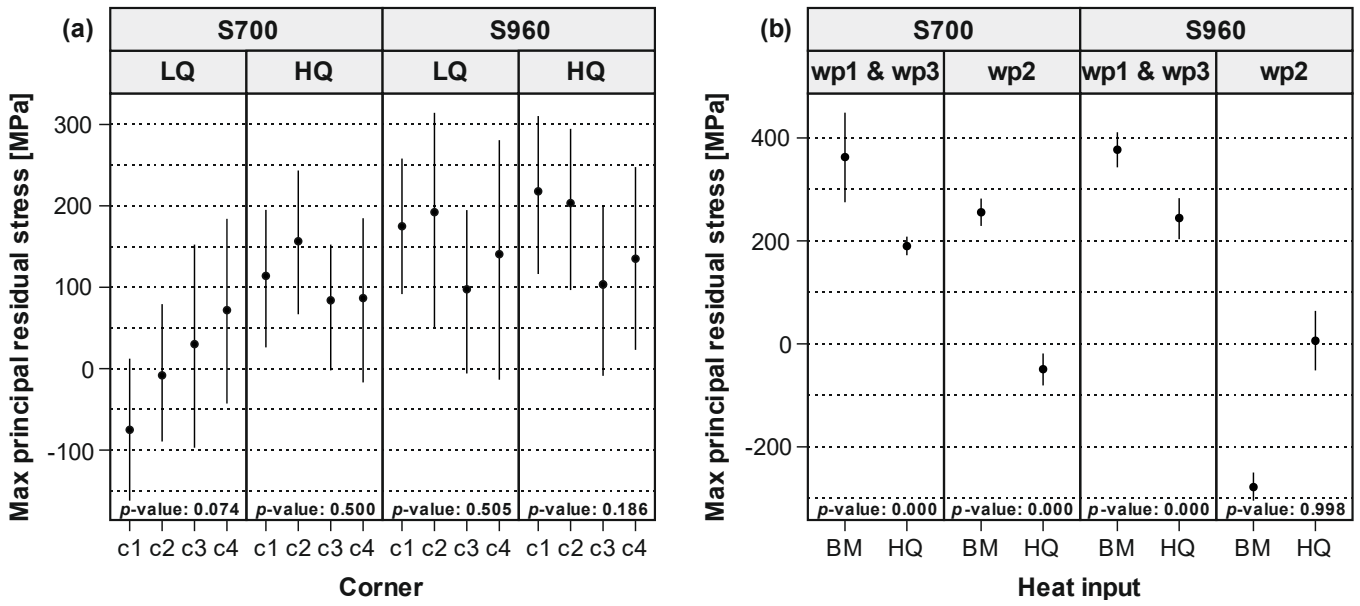

Fig. 11. Mean (black dots) of the maximum principal residual stresses with 95% confidence intervals (vertical lines through the dots) by a) corner and b) heat input.

concluded that the maximum principal stresses are not the same at the beginning and at the end of welding when steel grade S960 is welded with LQ heat input. The *p*-values greater than 0.05 for hypothesis tests 1, 2 and 4 indicate that welding direction has no significant effect on the maximum principal stresses in steel grade S700 and steel grade S960 welded with HQ heat input. This can clearly be seen in Fig. 10b, where a statistically significant difference between wp1 and wp3 can be observed for steel grade S960 with LQ heat input. It must be noted that the welding was performed by placing the rectangular hollow section corner upwards (see Fig. 1).

Table 9 summarizes the effect of welding sequence on the maximum principal stresses of welded hollow sections. All *p*-values for hypothesis tests 1–4 in Table 9 are greater than 0.05. This means that the welding sequence does not affect the minimum principal stress in any steel grade and heat input under study. The same behaviour of the maximum principal stresses is displayed in Fig. 11a. Although the mean values of the maximum principal stresses trend upwards in streel grade S700 with LQ heat input (the leftmost section in Fig. 11a), the hypothesis test cannot detect a difference between corners because the difference between means is small relative to their wide confidence intervals.

Table 10 summarizes the effect of welding heat input (HQ) on the maximum principal stresses at welding points wp1 & wp3 and wp2 compared to the unwelded rectangular hollow section, i.e, the base material (BM). The *p*-values of 0.000 of hypothesis tests $1-3$ in Table 10 indicate strong evidence against the assumptions; the heat input caused by welding reduces the maximum principal stresses to less than the corresponding stresses in the base material along the entire weld in steel grade S700 and at the beginning and at the end of welding in steel grade S960. The same phenomenon can clearly be seen in the three leftmost sections of Fig. 11b. This may be due to hollow section cold roll forming, which causes high residual stresses on the hollow section corners. The *p*-value of 0.998 for hypothesis test 4 in Table 10 shows that when using steel grade S960 and considering wp2, the maximum principal stresses in the base material are lower than in the welded material. The same conclusion can be drawn from the rightmost section of Fig. 11b. The results show that welding may relieve the situation in terms of residual stress state compared to unwelded tubes if compressive stresses are considered more desirable, except for corners of S960 steel. This is an important finding because components with lower welding residual stresses are safer to use in various fields of engineering. However, confirmatory studies may be needed with more variation in welding heat inputs and a larger number of specimens to draw more accurate conclusions.

3.4. FEM simulation

Abaqus software [40] was used to simulate the welding residual stresses of butt-welded hollow sections. Two simulation models were created for S700 and S960 steels depending on material properties and tube geometry. The models were calibrated based on the temperatures so that the melting temperature (~1500 °C) in the simulation model corresponds to the distance between fusion lines of welded specimens. The distances between fusion lines were about 6–8 mm for MAG-welded specimens; the molten area was narrower at the corners and wider on the flat sides of the MAG-welded RHS. The temperature distribution for S700 HQ during welding simulation is shown in Fig. 12a, where the maximum width of the grey area is about 7 mm and corresponds to the melted area in welded specimens. The example of maximum principal residual stress distribution after 1000 s cooling time is shown in Fig. 12b for S700 with HQ heat input.

The surface residual stresses of unwelded tube were set as initial residual stress states over the whole plate thickness in Abaqus. Because the initial stress is the same on the top and bottom surfaces, the simulated welding residual stresses on both surfaces seems to correspond to the measured residual stresses. However, on the thin layer of the top surface at the corner, the simulated residual stress is unrealistic and compressive. This may be due to the welding modelling technique or boundary conditions used. Thus, the results of the simulated corner are plotted from the inner side of the RHS, and they are in good agreement with the measurements, as shown in Fig. 13a and b.

Residual stress simulation results for S700 and S960 RHS with HQ welding heat input are shown in Fig. 13a and b, respectively. Residual stresses in Fig. 13 are presented as maximum principal residual stresses as a function of distance from the weld centre line. Based on the simulation and microstructure analyses, the peak values of tensile residual stress are close to the fusion line and coarse grained HAZ, where the heat has affected the material most strongly. Because the collimator size in the measurements was 3 mm, the measurement area includes both smaller and higher residual stresses. This is reflected in lower measured values compared to the simulation, as shown in Fig. 13. However, the obtained simulation results of mean values with confidence intervals correspond well to the measurements. The 95% confidence intervals

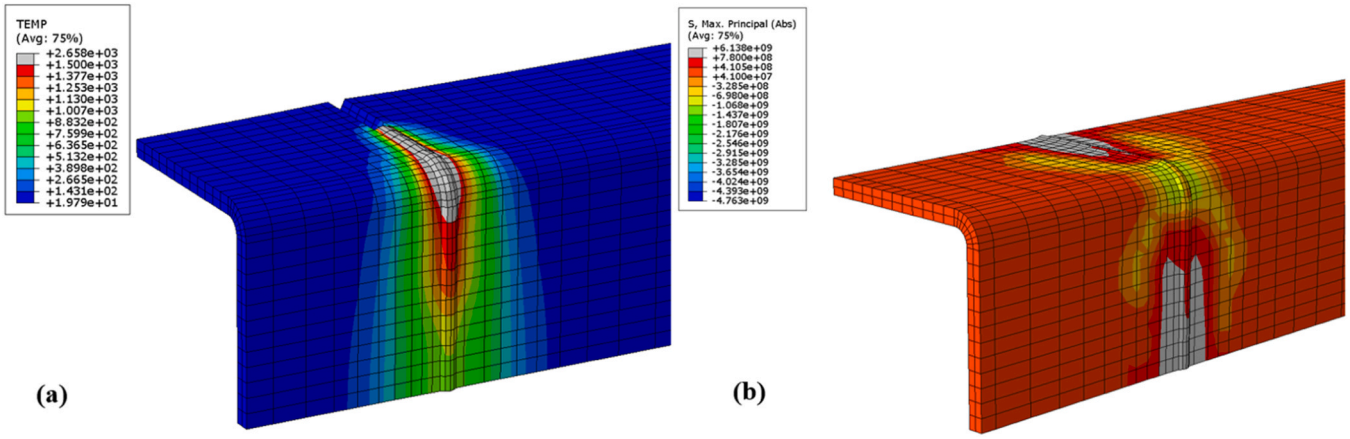

Fig. 12. Temperature distribution during simulation for S700 HQ; temperatures on grey areas are over 1500 °C (a) and simulated maximum principal residual stresses after cooling down for S700 HQ; surface stresses on grey areas exceeding the nominal yield strength (b).

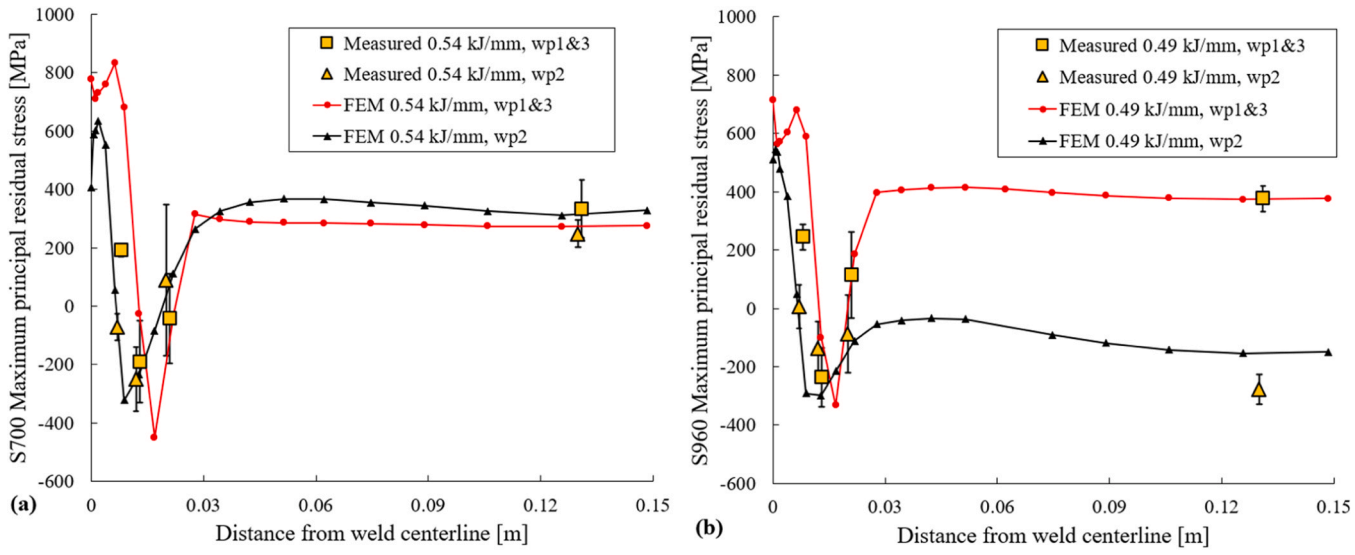

Fig. 13. Residual stresses from FEM simulation and measurements for S700 (a) and S960 (b) RHS. FEM results were read from the inner surface of the hollow sections.

were calculated based on Student's t-distribution. For S700 RHS, the peak residual stress is about 830 MPa while the room temperature yield strength is about 780 MPa. However, the peak value for S960 is only about 700 MPa while yield strength is 1050 MPa. For other cases, the residual stresses of S960 do not seem to be significantly higher than in S700. The simulation model also seems to predict the compressive residual stresses of S960 corner areas (wp2) moderately. It can therefore be concluded that the applied FEM model with the real measured material properties and initial residual stresses works well in the assessment of welding residual stresses in UHSS rectangular hollow sections.

Different simulation models were tested during the modelling phase. For example, the complete hollow section model yields similar results to the quarter model, but the calculation time greatly increased. Based on the optimized FEM model with a relatively small element number 2856, a short calculation time of 22 min and results corresponding to the measurements, it can be concluded that the proposed quarter model is computationally efficient and gives accurate results. In the literature, noticeably higher calculation times are reported: up to 165 h with 76000 elements for a longitudinal pipe weld [48] and 2 h with 2940 elements for a 300 mm butt-weld [49].

3.5. Residual stress prediction

Based on the statistical analysis, the welding direction and welding sequence do not significantly affect the residual stress formation of welded tube corners. Differences can only be found for lower heat input in S960 tubes. In the general case, we can therefore assume that all welded corners are similar regardless of welding sequence and direction. If the tube were welded with one uniform girth weld, the residual stress state will probably be different, and the proposed model will not fit the situation.

The relationship between welding heat input and maximum principal residual stresses can be predicted based on FEM simulations. The most important residual stresses are their local maximum values as maximum tensile (positive) and maximum compressive (negative, minimum stress) stresses, because they have the most significant effect on the mean stress in design situations. Especially the tensile residual stress is more important, degrading fatigue resistance of the welded joint. Local maximum values can be predicted as a function of welding heat input based on simulation results and curve fitting - logarithmic fit in this case. The local maximum values of measured and simulated maximum principal residual stresses from outside the fusion lines are shown in Fig. 14 along with prediction lines. The corresponding fitting

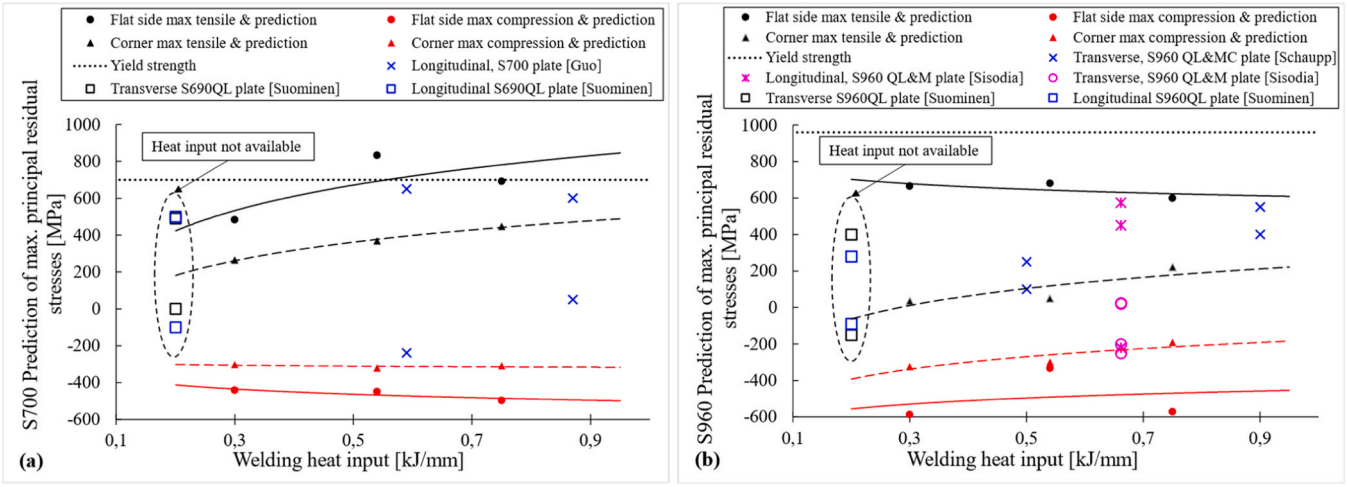

Fig. 14. Prediction of maximum and minimum values of residual stresses based on welding heat input outside of weld fusion lines for S700 (a) and S960 (b) RHS, and comparison with stresses of welded plates from the literature.

parameters with R-square values are shown in Table 11 for S700 and S960 RHS. The proposed prediction models are based on logarithmic curve fitting according to Eq. 1:

$$\sigma_{res,mp} = a \cdot \ln(Q) + b, \quad (1)$$

where $\sigma_{res,mp}$ is maximum principal residual stress, Q is welding heat input and a and b are parameters for the model shown in Table 11. Based on the R-square values in Table 11, the fitted logarithmic curves seems to predict residual stresses moderately for heat inputs ranging from 0.3 to 0.75 kJ/mm. The accuracy of the model and correlation between the fitted curve and the results could be improved with more different welding heat input values. It should be noted that if the fitting based on limited data do not show a clear upward or downward trend, the R-square may remain low even if the points are close to the fitted curve.

As shown in Fig. 14, the maximum residual stresses on the flat side of RHS, for both S700 and S960 steels, are a similar level. For S700 steel, the maximum values increase when heat input increases, while for S960 steel, the maximum stress level remains almost constant. At the corner, tensile residual stresses of S700 steel are higher that they are for S960 steel and stress level increases with heat input. When the residual stresses are compared with the nominal yield strengths, it can be seen that butt-welded S700 steel has higher tensile residual stresses in relation to yield strength. With higher heat inputs, the residual stresses on flat sides may even exceed the nominal yield strength for S700 steel. In the case of S960 steel, tensile residual stresses seem to be less than 75% of the nominal yield strength. When comparing residual stresses and yield strength, it should be noted that real measured yield strengths are about 800 MPa and 1050 MPa for S700 and S960 steels, respectively. Based on the results and proposed models, it can be said that the maximum compressive stresses (maximum negative values) cannot change to tensile in applicable heat input ranges, as shown in Fig. 14 by the red lines.

Residual stresses of butt welded high and ultra-high strength steel plates has been reported in the literature. For example, Guo et al. [50], Suominen et al. [51] Sisodia et al. [52] and Schaupp et al. [53] reported results for S690, S700 and S960 grade steels in the residual stress range of the proposed prediction model. These maximum and minimum residual stresses adjacent to the weld area are compared with the proposed residual stress prediction models. As shown in Fig. 14, the results from the literature are located between the prediction curves of maximum tensile and maximum compression residual stresses. Based on the comparison, the proposed models are suitable for estimating the maximum range of maximum principal residual stresses.

4. Conclusions

The effects of welding heat input on the microstructure and residual stresses in S700 and S960 butt-welded cold roll formed rectangular hollow sections caused by MAG-welding were studied. Based on microstructure research, comprehensive XRD measurements, statistical analyses and FEM simulations, a novel analytical model for predicting the heat input effects on studied rectangular hollow sections was proposed. The main results are summarized as follows:

- EBSD study revealed that the microstructures in the HAZ of cold-formed corner and flat sides are different and beyond 4 mm from the weld, the heat input seems to have no effect on the microstructure compared to the base material. The microstructures of studied steels are different; S700 is mainly polygonal ferrite and S960 consists of bainite. Based on the study, the microstructural changes should be considered when comparing the residual stresses caused by welding and hollow section manufacturing.
- Maximum principal residual stresses obtained from XRD measurements are typical for welded joints: tensile stress near to the weld, after that balancing compressive stress and then eventually back to base material levels. Generally, the obtained residual stresses due to welding are lower than from cold rolling, except for S960 corner areas where welding residual stresses increased. In addition, the

Table 11
Prediction parameters for Eq. (1).

		Max tensile residual stress			Max compression residual stress		
Steel	Area	a	b	R-square	a	b	R-square
S700	Flat side (wp1&3)	2.71E+ 08	8.60E+ 08	0.51	-5.49E+ 07	-5.02E+ 08	0.73
	Corner (wp2)	1.97E+ 08	8.60E+ 08	0.99	-1.52E+ 07	-3.03E+ 08	0.20
S960	Flat side (wp1&3)	-5.98E+ 07	6.07E+ 08	0.42	6.53E+ 07	-4.51E+ 08	0.45
	Corner (wp2)	1.83E+ 08	2.31E+ 08	0.66	2.92E+ 08	-4.26E+ 08	0.86

directions of maximum principal residual stresses were calculated: direction is parallel to weld in its vicinity and turns towards longitudinal to the tube in the base material. The change of residual stress direction should be noted when designing the most critical and highly variable-loaded welded joints.

- Based on the statistical analysis, between applied heat inputs, HQ only produced statistically significantly higher residual stresses compared to LQ for S700. For S960, the differences between HQ and LQ were not significant even though the mean values were different. From the welding direction and sequency point of view, there is only a significant effect with lower heat input in S960 steel, and correctly selected welding sequency does not affect the residual stresses of rectangular hollow section corners. Finally, there is statistical support for welding decreasing the tensile residual stress in both S700 and S960 steels, except for S960 in corner rounding with compressive residual stress.
- Based on the FEM simulations, the quarter model with symmetry boundary conditions can be used in residual stress prediction on butt-welded UHSS rectangular hollow sections. The base material residual stresses, as stresses from hollow section manufacturing, should be noted as predefined stresses in FEM calculations of welding residual stresses. When the material properties of welding heat input and initial state of the simulated material are considered, the applied weld segment model optimized for calculation time gives reasonably accurate results compared to measurements.
- Finally, the effect of welding heat input on residual stresses in corners and flat sides of S700 and S960 rectangular hollow sections were clarified by the FEM model. According to the simulation results, novel analytical prediction models were proposed based on curve fitting between welding heat input ranging from 0.35 to 0.75 kJ/mm for S700 and S960.
- Further research on UHSS rectangular hollow section residual stresses in the direction of thickness and on the inner surface using shell elements and the effects of different cross section could lead to more effective FEM models and eventually make the design of ultrahigh-strength steel structures where residual stresses play a major role easier.

CRediT authorship contribution statement

Lassi Keränen: Conceptualization, Methodology, Validation, Investigation, Visualization, Formal analysis, Writing-original draft, **Mika Pylvänäinen**: Conceptualization, Methodology, Investigation, Visualization, Formal analysis, Writing-original draft, **Antti Kaijalainen**: Methodology, Investigation, Visualization, Formal analysis, Writing-original draft, Tuomas Jokiaho: Investigation, Supervision, **Juha Tulonen**: Investigation, Supervision, **Anssi Hyvärinen**: Investigation, Supervision, **Minnamari Vippola**: Supervision, Project administration, **Emil Kurvinen**: Supervision, Project administration.

Declaration of Competing Interest

The authors declare that they have no known competing financial interests or personal relationships that could have appeared to influence the work reported in this paper.

Data availability

No data was used for the research described in the article.

Acknowledgements

The authors are grateful for financial support from the European Regional Development Fund, project OYH2– Hydrogen tank for Hydrogen Research at University of Oulu (A78681). Financial assistance of the Business Finland, project FOSSA– Fossil-Free Steel Applications (Dno 5397/31/2021), is acknowledged. The authors are also grateful to the machine shop and Process Metallurgy unit of the University of Oulu and Tampere University for help with specimen preparation, heat capacity measurements and residual stress measurements.

Appendix

Maximum principal residual stresses of butt-welded and unwelded S700 and S960 RHS are shown in Table 1. A and 2. A, respectively. Two welded specimens were measured at 2 mm from the butt-weld.

Table A1
Residual stresses of welded and unwelded S700 tubes at different distances from the weld.

Specimen				Maximum principal stress [MPa]				
	Corner	Number	Welding point	2 mm (A)	2 mm (B)	7 mm (A)	15 mm (A)	125 mm, BM (A)
700 HQ	c1	1	1	187.9	192.3	-216.2	31.8	227.8
	c1	2	2	-64.6	-24.6	-215.6	275.6	240.0
	c1	3	3	187.2	205.6	2.6	0.0	195.3
	c4	4	3	151.1	159.3	-149.7	-72.8	334.9
	c4	5	2	-80.4	-113.2	-173.7	119.8	218.1
	c4	6	1	186.5	216.7	89.2	264.3	224
	c2	7	1	262	238.3	-344.7	-160.0	486.2
	c2	8	2	-17.9	-1.4	-325.1	83.7	244.6
	c2	9	3	218.1	240.1	-350.8	-120.4	488.7
	c3	10	3	127.2	159.2	-193.1	-354.5	528.4
	c3	11	2	-104.1	-159.7	-289.5	-119.8	289.8
	c3	12	1	148.6	159.9	-366.0	74.5	417.4
700 LQ	c1	1	1	-222.9	-204.2	-342.0	-316.2	
	c1	2	2	-58.4	-60.5	-354.9	-137.9	
	c1	3	3	110.1	-14.8	-261.3	-60.8	
	c4	4	3	131	136.3	-136.4	268.0	
	c4	5	2	-140.4	-119.2	-263.5	49.6	
	c4	6	1	190	233.6	-291.5	-275.6	
	c2	7	1	157	-93.4	-326.5	-78.3	
	c2	8	2	-69.6	-14.8	-438.9	-61.9	
	c2	9	3	-138	109.5	-380.8	-198.4	

(*continued on next page*)

Table A1 (*continued*)

Specimen				Maximum principal stress [MPa]				
	Corner	Number	Welding point	2 mm (A)	2 mm (B)	7 mm (A)	15 mm (A)	125 mm, BM (A)
	c3	10	3	39.2	124.8	-174.4	16.3	
	c3	11	2	-162.5	-193.3	-454.0	-362.6	
	c3	12	1	120	252.7	-302.9	-123.1	

Table A2
Residual stresses of welded and unwelded S960 tubes at different distances from the weld.

Specimen				Maximum principal stress [MPa]				
	Corner	Number	Welding point	2 mm (A)	2 mm (B)	7 mm (A)	15 mm (A)	125 mm, BM (A)
960 HQ	c1	1	1	333.9	325.3	-301.5	-233.3	313.7
	c1	2	2	93.0	11.4	-82.4	17.1	-314.9
	c1	3	3	244.9	298.4	-28.9	218.2	376.1
	c4	4	3	298.4	133.2	-148.3	203.9	382.2
	c4	5	2	39.8	-84.9	-102.0	-77.8	-237.9
	c4	6	1	328.3	95.6	-154.2	164.9	429.5
	c2	7	1	328.2	175.5	-326.3	-76.0	447.0
	c2	8	2	147.1	-25.7	-157.5	-186.3	-286.3
	c2	9	3	254.7	340.4	-230.1	254.9	420.4
	c3	10	3	172	137	-408.5	117.2	331.2
	c3	11	2	-5.1	-128	-212.3	-100.0	-273.8
	c3	12	1	276.9	168.1	-292.9	262.4	316.4
960 LQ	c1	1	1	343.6	159.2	-269.2	70.9	
	c1	2	2	185.2	1.8	-95.8	-152.1	
	c1	3	3	-	209.4	-216.0	279.5	
	c4	4	3	201.0	172.4	-403.7	-174.5	
	c4	5	2	-2.1	-195.4	-259.8	-315.7	
	c4	6	1	350.3	317.8	-331.6	83.9	
	c2	7	1	351.2	375.2	-248.3	191.6	
	c2	8	2	113.2	-95.2	-156.2	-130.9	
	c2	9	3	120.3	288.5	-269.6	266.5	
	c3	10	3	111.9	151.3	-406.6	-144.0	
	c3	11	2	-7.3	-103.4	-276.0	-291.5	
	c3	12	1	131	301.3	-452.2	-195.4	

The directions of maximum principal residual stresses of butt-welded and unwelded S700 and S960 are shown in Table 1. A and 2. A, respectively. Direction in the Tables is difference from butt weld longitudinal direction.

Table A3
Residual stress direction of welded and unwelded S700 RHS at different distances from the weld.

Specimen				Direction of maximum principal stress from butt-weld [°]				
	Corner	Number	Welding point	2 mm (A)	2 mm (B)	7 mm (A)	15 mm (A)	125 mm, BM (A)
700 HQ	c1	1	1	6	3.6	16.9	50.4	89
	c1	2	2	6.1	0.4	9.9	78.7	72.1
	c1	3	3	74.2	10	82.9	60.7	70.7
	c4	4	3	12.9	6.4	29.5	61.9	88.4
	c4	5	2	1.3	0.2	3.3	45	81.7
	c4	6	1	9.1	9.8	20.5	13.7	49.8
	c2	7	1	0.2	0.7	4.5	31.5	80.4
	c2	8	2	4.1	0.7	3.3	31.1	62.4
	c2	9	3	10.2	7.2	22.8	70.7	74.1
	c3	10	3	10.7	9.2	27.4	70.3	80.6
	c3	11	2	2.9	2	2.2	28.5	62.2
	c3	12	1	8.8	11.4	24	46.8	67.4
700 LQ	c1	1	1	5.6	6.70	10.2	25.6	
	c1	2	2	5.4	3	29.8	81.8	
	c1	3	3	8.1	11	11.4	80.5	
	c4	4	3	10	7	18.2	64.3	
	c4	5	2	0	0.1	0.9	69	
	c4	6	1	9	9.8	12.1	55.7	
	c2	7	1	2	3.7	1.5	64.6	
	c2	8	2	0.5	2.5	5.3	48.7	
	c2	9	3	2.7	4.5	2.1	2.6	
	c3	10	3	4.7	9.5	37.5	84.1	
	c3	11	2	1.1	1.5	5.3	10.2	
	c3	12	1	7.2	9.3	20.7	65.6	

Table A4
Residual stress direction of welded and unwelded S960 RHS at different distances from the weld.

Specimen				Direction of maximum principal stress from butt-weld [°]				
	Corner	Number	Welding point	2 mm (A)	2 mm (B)	7 mm (A)	15 mm (A)	125 mm, BM (A)
960 HQ	c1	1	1	4.7	4.5	18.4	40.3	83.6
	c1	2	2	0.8	12.3	1.7	75.1	3.2
	c1	3	3	4.0	2.6	40	41.8	89.5
	c4	4	3	1.1	4.4	28	53.9	83.9
	c4	5	2	0.1	5.1	1.5	7	66.5
	c4	6	1	1.5	7.7	9.5	83.3	81.9
	c2	7	1	5.6	3.4	16.2	86.3	81.9
	c2	8	2	13.9	4.3	10.7	25	17.4
	c2	9	3	2.8	1.5	21.2	58.1	87
	c3	10	3	1	3.4	36	58.3	75.1
	c3	11	2	5.3	2.4	0.2	3.4	20.7
	c3	12	1	9	11	17.6	88.4	83.4
960 LQ	c1	1	1	0.7	2.6	36.4	68.1	
	c1	2	2	14.8	13.9	29.9	60.4	
	c1	3	3	-	3.8	59.3	82.7	
	c4	4	3	0.2	0.4	20.2	54.1	
	c4	5	2	5	4.8	0.7	3	
	c4	6	1	8.4	8.5	21.6	83.6	
	c2	7	1	7.2	4.4	25	81.6	
	c2	8	2	9.5	10	3.4	7.3	
	c2	9	3	1.6	0.7	20	81.4	
	c3	10	3	0.7	3.6	53.2	48.6	
	c3	11	2	7.3	9.1	2.6	0.9	
	c3	12	1	1.3	9	24.3	78.1	

During the preparation of this work the corresponding author used OpenAI ChatGPT in order to improve the fluency and quality of the Abstract in this paper. After using this tool, the authors reviewed and edited the content as needed and takes full responsibility for the content of the publication.

References

[1] Norton RL. Machine design. 2. ed..,. NJ: Prentice Hall, Upper Saddle River,; 2000.
[2] Hobbacher AF. Recommendations for Fatigue Design of Welded Joints and Components. 2nd ed..,. Springer International Publishing; 2016. https://doi.org/10.1007/978-3-319-23757-2.
[3] Ghafouri M, Ahola A, Ahn J, Björk T. Numerical and experimental investigations on the welding residual stresses and distortions of the short fillet welds in high strength steel plates. Eng Struct 2022;260:114269. https://doi.org/10.1016/J.ENGSTRUCT.2022.114269.
[4] Keränen L, Nousiainen O, Javaheri V, Kaijalainen A, Pokka AP, Keskitalo M, et al. Mechanical properties of welded ultrahigh-strength S960 steel at low and elevated temperatures. J Constr Steel Res 2022;198. https://doi.org/10.1016/j.jcsr.2022.107517.
[5] Barsoum Z, Barsoum I. Residual stress effects on fatigue life of welded structures using LEFM. Eng Fail Anal 2009;16:449–67. https://doi.org/10.1016/J.ENGFAILANAL.2008.06.017.
[6] Krebs J, Kassner M. Influence of welding residual stresses on fatigue design of welded joints and components. Weld World 2007;51:54–68. https://doi.org/10.1007/BF03266586.
[7] Deng D. FEM prediction of welding residual stress and distortion in carbon steel considering phase transformation effects. Mater Des 2009;30:359–66. https://doi.org/10.1016/J.MATDES.2008.04.052.
[8] Yan R, Yu Z, Wang S, Liu J. Influence of welding residual stress on bending resistance of hollow spherical joints. J Constr Steel Res 2023;208:108004. https://doi.org/10.1016/J.JCSR.2023.108004.
[9] Sun J, Dilger K. Reliability analysis of thermal cycle method on the prediction of residual stresses in arc-welded ultra-high strength steels. Int J Therm Sci 2023;185:108085. https://doi.org/10.1016/J.IJTHERMALSCI.2022.108085.
[10] Radaj Dieter. Heat Effects of Welding: Temperature Field, Residual Stress, Distortion. 1st ed..,. Heidelberg: Springer Berlin; 1992. https://doi.org/10.1007/978-3-642-48640-1.
[11] Goldak JA, Akhlaghi M. Computational Welding Mechanics. Springer; 2005.
[12] Teng TL, Chang PH, Tseng WC. Effect of welding sequences on residual stresses. Comput Struct 2003;81:273–86. https://doi.org/10.1016/S0045-7949(02)00447-9.
[13] Deng D, Kiyoshima S, Ogawa K, Yanagida N, Saito K. Predicting welding residual stresses in a dissimilar metal girth welded pipe using 3D finite element model with a simplified heat source. Nucl Eng Des 2011;241:46–54. https://doi.org/10.1016/J.NUCENGDES.2010.11.010.
[14] Hu L, Li X, Luo W, Li S, Deng D. Residual stress and deformation in UHS quenched steel butt-welded joint. Int J Mech Sci 2023;245:108099. https://doi.org/10.1016/J.IJMECSCI.2023.108099.
[15] Ghafouri M, Ahn J, Mourujärvi J, Björk T, Larkiola J. Finite element simulation of welding distortions in ultra-high strength steel S960 MC including comprehensive thermal and solid-state phase transformation models. Eng Struct 2020;219:110804. https://doi.org/10.1016/J.ENGSTRUCT.2020.110804.
[16] Knoedel P, Gkatzogiannis S, Ummenhofer T. Practical aspects of welding residual stress simulation. J Constr Steel Res 2017;132:83–96. https://doi.org/10.1016/J.JCSR.2017.01.010.
[17] Vemanaboina H, Akella S, Buddu RK. Welding process simulation model for temperature and residual stress analysis. Procedia Mater Sci 2014;6:1539–46. https://doi.org/10.1016/J.MSPRO.2014.07.135.
[18] Xiao M, Hu YF, Jin H, Chung KF, Nethercot DA. Prediction of residual stresses in high-strength S690 cold-formed square hollow sections using integrated numerical simulations. Eng Struct 2022;253:113682. https://doi.org/10.1016/J.ENGSTRUCT.2021.113682.
[19] Bhatti AA, Barsoum Z, Murakawa H, Barsoum I. Influence of thermo-mechanical material properties of different steel grades on welding residual stresses and angular distortion. Mater Des (1980-2015) 2015;65:878–89. https://doi.org/10.1016/J.MATDES.2014.10.019.
[20] Li SH, Zeng G, Ma YF, Guo YJ, Lai XM. Residual stresses in roll-formed square hollow sections. Thin-Walled Struct 2009;47:505–13. https://doi.org/10.1016/J.TWS.2008.10.015.
[21] Somodi B, Kövesdi B. Residual stress measurements on cold-formed HSS hollow section columns. J Constr Steel Res 2017;128:706–20. https://doi.org/10.1016/J.JCSR.2016.10.008.
[22] Abathun MZ, Han J, Yu W. Effects of manufacturing methods and production routes on residual stresses of rectangular and square hollow steel sections: a review. Arch Civ Mech Eng 2021;21:1–19. https://doi.org/10.1007/s43452-021-00193-8.
[23] Yao Y, Quach WM, Young B. Finite element-based method for residual stresses and plastic strains in cold-formed steel hollow sections. Eng Struct 2019;188:24–42. https://doi.org/10.1016/J.ENGSTRUCT.2019.03.010.
[24] Jaamala L, Mela K, Laurila J, Rinne M, Peura P. Probabilistic modelling of residual stresses in cold-formed rectangular hollow sections. J Constr Steel Res 2022;189:107108. https://doi.org/10.1016/J.JCSR.2021.107108.
[25] Ma J-L, Chan T-M, Young B. Material properties and residual stresses of cold-formed high strength steel hollow sections. J Constr Steel Res 2015;109. https://doi.org/10.1016/j.jcsr.2015.02.006.
[26] Kaijalainen A, Mourujärvi J, Tulonen J, Steen P, Kömi J. Effect of ageing on the mechanical properties of cold formed S700 rectangular hollow. IOP Conf Ser Mater Sci Eng 2021. https://doi.org/10.1088/1757-899X/1178/1/012026.
[27] Core Team, R: A language and environment for statistical computing. R Foundation for Statistical Computing, Vienna, Austria., Https://Www.R-Project.Org/ (2023).
[28] Efron B. Bootstrap methods: another look at the jackknife. Ann Stat 1979;7. https://doi.org/10.1214/aos/1176344552.
[29] Bradley Efron, Robert Tibshirani. An introduction to the bootstrap. 1st ed..,. Chapman & Hall; 1993.

[30] Janssen A. Studentized permutation tests for non-i.i.d. hypotheses and the generalized Behrens-Fisher problem. Stat Probab Lett 1997;36:9–21. https://doi.org/10.1016/S0167-7152(97)00043-6.
[31] Chung E, Romano JP. Exact and asymptotically robust permutation tests. Ann Stat 2013;41:484–507. https://doi.org/10.1214/13-AOS1090.
[32] Manly BFJ, Alberto JANavarro. Random, Bootstrap Monte Carlo Methods Biol 2020. https://doi.org/10.1201/9780429329203.
[33] EN 10219–3, EN 10219–3:2020. Cold formed welded steel structural hollow sections. Part 3: Technical delivery conditions for high strength and weather resistant steels, 2020.
[34] SSAB, Welding of Strenx, 2017.
[35] European committee for standardization, SFS-EN 15305. Non-destructive Testing. Test Method fo Residual Stress analysis by X-ray Diffraction., 2008.
[36] Jokiaho T, Stress Residual. Microstructure and Cracking Characteristics of Flame Cut Thick Steel Plates - Towards Optimized Flame Cutting Practices, Academic Dissertation. Tampere University; 2019.
[37] Jokiaho T, Santa-Aho S, Järvinen H, Honkanen M, Peura P, Vippola M. Effect of Microstructural Characteristics of Thick Steel Plates on Residual Stress Formation and Cracking during Flame Cutting. Mater Perform Charact 2018;7:655–74. https://doi.org/10.1520/MPC20170083.
[38] Withers PJ, Turski M, Edwards L, Bouchard PJ, Buttle DJ. Recent advances in residual stress measurement. Int J Press Vessels Pip 2008;85:118–27. https://doi.org/10.1016/J.IJPVP.2007.10.007.
[39] Davison AC, Hinkley DV. Bootstrap methods and their application. 1st ed..,. New York: Cambridge University Press; 1997.
[40] Dassault Systemes, Abaqus CAE, (2019).
[41] Dassault Systemes, Abaqus Documentation: Heat transfer and thermal-stress analysis, (2019).
[42] Keränen L, Kangaspuoskari M, Niskanen J. Ultrahigh-strength steels at elevated temperatures. J Constr Steel Res 2021;183. https://doi.org/10.1016/j.jcsr.2021.106739.
[43] EN 1993–1-2, EN 1993–1-2. Eurocode 3: Design of steel structures. Part 1–2: Structural fire design., 2005.
[44] Nedoseka A. Fundamentals of evaluation and diagnostics of welded structures. Elsevier Ltd,; 2012. https://doi.org/10.1533/9780857097576.
[45] Dassault Systemès, Defining plasticity in Abaqus - SIMULIA User Assistance 2020, (2020). https://help.3ds.com/2020/english/dssimulia_established/SIMACAEGSARefMap/simagsa-c-matdefining.htm?contextscope=all&id=4b68b8a9702546b5b98f8b0265a1cf67 (accessed February 21, 2023).
[46] Yao Y, Quach WM, Young B. Finite element-based method for residual stresses and plastic strains in cold-formed steel hollow sections. Eng Struct 2019;188:24–42. https://doi.org/10.1016/J.ENGSTRUCT.2019.03.010.
[47] ASTM E1269–11, ASTM E1269–11. Standard Test Method for Determining Specific Heat Capacity by Differential Scanning Calorimetry, 2018. https://www.astm.org/e1269–11r18.html (accessed February 21, 2023).
[48] Hu YF, Chung KF, Ban H, Nethercot DA. Investigations into residual stresses in S690 cold-formed circular hollow sections due to transverse bending and longitudinal welding. Eng Struct 2020;219:110911. https://doi.org/10.1016/J.ENGSTRUCT.2020.110911.
[49] Mikihito H, Yoshito I. A simplified FE simulation method with shell element for welding deformation and residual stress generated by multi-pass butt welding. Int J Steel Struct 2016;16:51–8. https://doi.org/10.1007/S13296-016-3005-0/METRICS.
[50] Guo W, Francis JA, Li L, Vasileiou AN, Crowther D, Thompson A. Residual stress distributions in laser and gas-metal-arc welded high-strength steel plates. Mater Sci Technol 2016;32:1449–61. https://doi.org/10.1080/02670836.2016.1175687.
[51] Suominen L, Khurshid M, Parantainen J. Residual stresses in welded components following post-weld treatment methods. Procedia Eng 2013;66:181–91. https://doi.org/10.1016/j.proeng.2013.12.073.
[52] Sisodia RPS, Gáspár M, Sepsi M, Mertinger V. Comparative evaluation of residual stresses in vacuum electron beam welded high strength steel S960QL and S960M butt joints. Vacuum 2021;184:109931. https://doi.org/10.1016/j.vacuum.2020.109931.
[53] Schaupp T, Schroepfer D, Kromm A, Kannengiesser T. Welding residual stresses in 960 MPa grade QT and TMCP high-strength steels. J Manuf Process 2017;27:226–32. https://doi.org/10.1016/j.jmapro.2017.05.006.